

2023

## Feedback Control Methods on Short-Period Orbits Of the Earth-Moon Equilateral Libration Points

Luis E. Mendoza Zambrano

Franco Criscola

David Canales Garcia

Riccardo Bevilacqua

Stephen Eikenberry

*See next page for additional authors*

Follow this and additional works at: <https://commons.erau.edu/student-works>

---

This Article is brought to you for free and open access by Scholarly Commons. It has been accepted for inclusion in Student Works by an authorized administrator of Scholarly Commons. For more information, please contact [commons@erau.edu](mailto:commons@erau.edu).

---

**Authors**

Luis E. Mendoza Zambrano, Franco Criscola, David Canales Garcia, Riccardo Bevilacqua, Stephen Eikenberry, Octavi Fors, José María Gómez, and Andrea Richichi

## FEEDBACK CONTROL METHODS ON SHORT-PERIOD ORBITS OF THE EARTH-MOON EQUILATERAL LIBRATION POINTS

Luis E. Mendoza Zambrano\*, Franco Criscola\*, David Canales†, Riccardo Bevilacqua‡, Stephen Eikenberry§, Octavi Fors¶, José María Gómez||, Andrea Richichi\*\*

Recent research by the authors suggests a unique approach to perform Lunar occultations for a diverse set of scientific applications. Under the circular restricted three-body problem assumptions, short-period orbits (SPOs) near the Earth-Moon equilateral Libration points have been suggested for optimal eclipse time and minimal fuel consumption requirements to stay in orbit. Nevertheless, under the presence of orbital perturbations, SPOs are no longer stable as gravitational effects from neighboring celestial bodies continuously perturb these orbits. In this sense, the current study compares a wide range of control methods, including Lyapunov-based adaptive control schemes and fuel-optimal control policies, to address the fuel consumption and tracking issues of the perturbed system. This inquiry attests that perturbations are effectively cancelled out to achieve the proposed scientific objectives with minimal station-keeping requirements.

### INTRODUCTION

Preceding research by the authors proposes a novel approach to study Lunar occultations (LO) within the context of the circular restricted three-body problem (CR3BP).<sup>1,2</sup> Lunar occultations occur when the Moon passes between a light source and a spacecraft to allow for shadowing of its incident light. Some applications of LO include measurement of stellar angular diameters and the study of small separation binary stars and circumstellar material in the form of gas or dust envelopes; all of which correspond to key parameters in the study of stellar properties such as surface temperature, energy production, evolution, and formation.<sup>3</sup> Short-period orbits (SPOs) in the vicinity of the Earth-Moon equilateral Libration points have been suggested for maximum eclipse time with minimal station-keeping requirements while using the Moon as a natural occulter.<sup>1,2</sup> Additionally, a physical study of the benefits of pursuing LO from SPOs with respect to Earth has been presented,

\*PhD Student, Aerospace Engineering, Embry-Riddle Aeronautical University, 1 Aerospace Blvd, Daytona Beach, FL 32114, Email: mendol10@my.erau.edu.

†Assistant Professor, Aerospace Engineering, Embry-Riddle Aeronautical University, 1 Aerospace Blvd, Daytona Beach, FL 32114, Email: david.canalesgarcia@erau.edu, Website: <https://www.staresearchgroup.com>.

‡Professor, Aerospace Engineering, Embry-Riddle Aeronautical University, 1 Aerospace Blvd, Daytona Beach, FL 32114, Email: bevilacr@erau.edu, Website: <https://www.riccardobevilacqua.com>.

§Professor, College of Optics and Photonics, University of Central Florida, 4000 Central Florida Blvd, Orlando, FL 32816.

¶Dept. de Física Quàntica i Astrofísica, Institut de Ciències del Cosmos (ICCUB), Universitat de Barcelona, IEEC-UB, Martí i Franquès 1, Barcelona, E-08028, Spain.

||Dept. d'Enginyeria Electrònica i Biomèdica, Institut de Ciències del Cosmos (ICCUB), Universitat de Barcelona, IEEC-UB, Martí i Franquès 1, Barcelona, E-08028, Spain.

\*\*INAF - Osservatorio Astrofisico di Arcetri, Largo E. Fermi 5, 50125, Firenze, Italy.

proving the potential of a mission for astrophysical purposes. In particular, it was shown that observing LO from SPOs outperforms Earth-based observation, offering the potential to detect wavelengths below 250 nm with the absence of scintillation noise and slower diffraction fringes. It has also been demonstrated that this method allows for the best possible angular resolution in the near ultraviolet band.<sup>1,2</sup>

As it is commonly known from the literature, the equilateral Libration points  $L_4$  and  $L_5$  of the Earth-Moon system are stable under the CR3BP assumptions.<sup>4</sup> In this context, SPOs, particularly in the neighborhood of  $L_4$ , are suggested due to their minimal station-keeping requirements as well as their low angular velocities relative to the Moon to enhance the quality of LO.<sup>1,2,5</sup> However, substantial research on orbital control of SPOs near the equilateral Libration points has not been extensively addressed in the literature, as it is often misunderstood that these orbits are naturally stable. Furthermore, limited by the *state-of-the-art* in spacecraft navigation and support from governmental and private organizations, there has been no prospective missions considered, as this region of space is unoccupied by astronomical bodies of interest and sufficiently distant away from Earth. Nevertheless, significant research on the unstable and colinear Libration points of the Earth-Moon system is conveniently found in the literature. For instance, in Reference 6, a long-term station-keeping strategy is addressed specifically for the colinear Libration points  $L_1$  and  $L_2$ . Here, different trajectory segments are used to target a set of terminal conditions and path constraints. Similarly, in Reference 7, a modified targeting strategy is developed based on the dynamic property of the state transition matrix. More in detail, results are presented for a set of Lyapunov and Halo orbits, as well as periodic orbits around  $L_4$ , in terms of average time between maneuvers and fuel consumption while considering major orbital perturbations. Nonetheless, the results in these papers are not intended to address the required tolerance of the eclipse zone to perform LO.

In the presence of perturbations, SPOs are no longer stable as gravitational effects from neighboring celestial bodies continuously perturb these orbits. In this inquiry, an extensively diverse set of control methods are evaluated in terms of fuel consumption and tracking to explore different solutions to the perturbed system. Conventional linear-optimal state-feedback control policies and Lyapunov-based adaptive control schemes are considered in addition to a nonlinear dynamic programming control sequence using *GPOPS-II* along with an interior-point optimizer *IPOPT*.<sup>8</sup> More in detail, the current study examines and compares the implementation of a model reference adaptive control (MRAC) architecture with disturbance rejection as well as an  $\mathcal{L}_1$ -type adaptive control policy, which initially suggests better performance and robustness under the presence of unknown perturbations.<sup>9,10</sup> In addition, a perturbation model, compatible with the Earth-Moon rotating frame of the CR3BP, is addressed in this paper to allow for testing of the numerous control schemes proposed previously.

The paper is organized as follows. First, the CR3BP is introduced. Consequently, the perturbation model, that considers the gravitational pull of the Sun, the eccentricity effect of the orbit of the Moon, and Solar radiation pressure, is presented. Then, a linear quadratic (LQ) control policy is described to track the unperturbed reference trajectory. Next, a Lyapunov-based adaptive control scheme with disturbance rejection is derived and further modified with an  $\mathcal{L}_1$ -type adaptive control architecture to estimate unknown perturbations. Subsequently, a fuel-optimal nonlinear dynamic programming control problem is formulated for comparison. Finally, numerical simulations in the results and discussion section show the contribution of this work along with prominent conclusions for upcoming future work.

## THE CIRCULAR RESTRICTED THREE-BODY PROBLEM

Assuming the Moon orbits the Earth along a circular orbit, the equations of motion of a spacecraft are described by the following set of non-dimensional equations as seen by a synodic observer whose origin lies at the Earth-Moon barycenter (see Figure 1). Here, we assume the mass of the spacecraft is infinitesimally small compared to the two primary bodies.<sup>11</sup>

$$\ddot{x} - 2\dot{y} = \frac{\partial U^*}{\partial x} \quad \ddot{y} + 2\dot{x} = \frac{\partial U^*}{\partial y} \quad \ddot{z} = \frac{\partial U^*}{\partial z} \quad (1)$$

where  $U^*$  is the pseudo-potential function of the Earth-Moon system.<sup>11</sup>

$$U^* \triangleq \frac{1-\mu}{r_{e-s/c}} + \frac{\mu}{r_{m-s/c}} + \frac{1}{2}(x^2 + y^2) \quad (2)$$

Henceforth,  $\mu \triangleq m_m/(m_e + m_m)$  is the mass ratio of the system where  $m_e$  and  $m_m$  denote the mass of the Earth and Moon, respectively. Then,  $r_{e-s/c}$  is the instantaneous non-dimensional Earth-spacecraft distance and  $r_{m-s/c}$  denotes the instantaneous non-dimensional distance of the spacecraft to the Moon, both represented as follows:

$$r_{e-s/c} = \sqrt{(x + \mu)^2 + y^2 + z^2} \quad r_{m-s/c} = \sqrt{(x - 1 + \mu)^2 + y^2 + z^2} \quad (3)$$

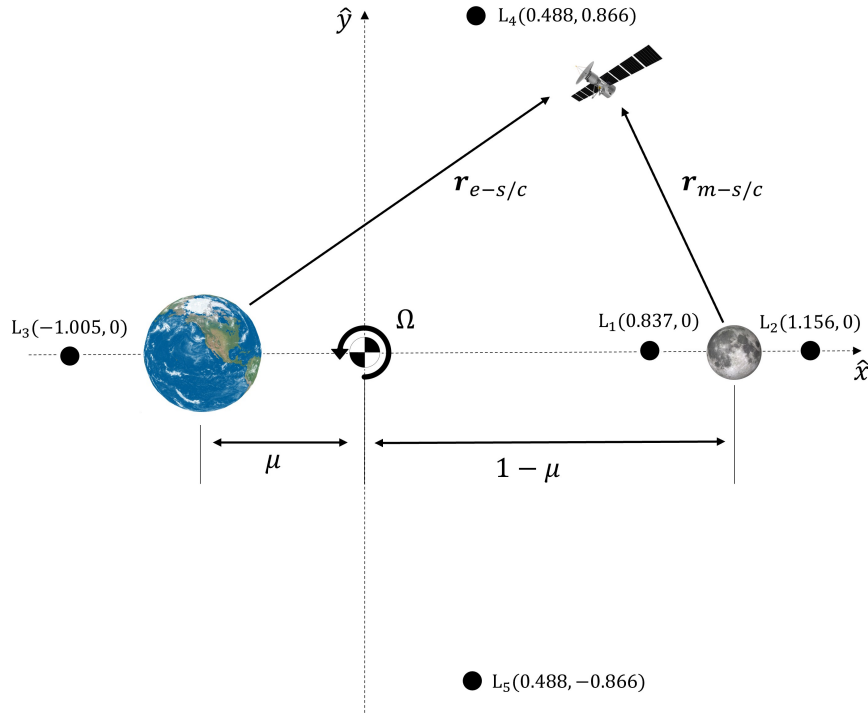


Figure 1. Earth-Moon Synodic Frame in Non-Dimensional Coordinates (Not to Scale).

The dimensional position and velocity vectors of the spacecraft are easily retrieved given the characteristic quantities of the Earth-Moon system.<sup>11</sup>

$$l^* \triangleq r_{e-m} \quad m^* \triangleq m_e + m_m \quad t^* \triangleq \sqrt{\frac{l^{*3}}{Gm^*}} \quad v^* \triangleq \frac{l^*}{t^*} \quad (4)$$

where  $r_{e-m}$  represents the Earth-Moon distance and  $G$  denotes the gravitational constant. For explicitness,  $l^*$  and  $m^*$  are commonly referred to as the characteristic length and mass of the Earth-Moon system, respectively. Similarly,  $t^*$  and  $v^*$  are introduced as the characteristic time and velocity of the CR3BP. From this formulation, one can derive the equilibrium points, often called Libration or Lagrange points, that denote the location in space where the velocity and acceleration of the spacecraft are zero. Three collinear points,  $L_1$ ,  $L_2$ , and  $L_3$ , along the Earth-Moon vector indicate unstable equilibrium points (see Figure 1), while the remaining two,  $L_4$  and  $L_5$ , constitute the stable equilibria of interest of this study from where SPOs are found.<sup>4</sup>

## PERTURBATION MODEL

Periodic motion within the neighborhood of the Earth-Moon equilateral Libration points is stable owing to CR3BP assumptions. In this formulation, orbital perturbations are neglected. Therefore, in an attempt to illustrate the need to account for such perturbations, the gravitational effects from the Sun and the eccentricity of the orbit of the Moon are modeled in addition to Solar radiation pressure within the framework of the CR3BP. The presence of Kordylewski clouds is not considered in the perturbation model due to our limited knowledge to quantify its effect; nevertheless, future research should consider modeling Kordylewski clouds as more observations are made to understand their physics.<sup>12</sup>

### Gravitational Pull of the Sun

The bi-circular restricted four-body problem (BCR4BP), introduced as a perturbed variation of the CR3BP,<sup>13</sup> describes the gravitational effect of the Sun, assuming circular motion around the Earth-Moon barycenter. Furthermore, the  $5.15^\circ$  inclination of the orbit of the Moon relative to the ecliptic plane is neglected in the original formulation, as it is assumed that the plane of motion of the Sun is co-planar to the synodic plane. In this formulation, the Earth and the Moon are still assumed to move along circular orbits around their common barycenter.<sup>13</sup> In this sense, the CR3BP equations of motion are modified to include the gravitational effect of the Sun as follows:

$$\ddot{x} = 2\dot{y} + \frac{\partial \Lambda^*}{\partial x} \quad \ddot{y} = -2\dot{x} + \frac{\partial \Lambda^*}{\partial y} \quad \ddot{z} = \frac{\partial \Lambda^*}{\partial z} \quad (5)$$

where  $\Lambda^*$  is the pseudo-potential that includes the non-dimensional gravitational effect of the Sun.<sup>13</sup>

$$\Lambda^* \triangleq U^* + \frac{\mu_s}{r_{s-s/c}} - \frac{\mu_s}{a_s^3}(x_s x + y_s y + z_s z) \quad (6)$$

Here,  $\mathbf{a}_s = [x_s \ y_s \ z_s]^T$  is the non-dimensional position vector of the Sun as viewed by a synodic observer, while  $a_s \triangleq \|\mathbf{a}_s\|$  denotes its euclidean norm. Also, note that  $\mu_s \triangleq m_s/m^*$  is the non-dimensional mass of the Sun while  $r_{s-s/c}$  is the non-dimensional distance of the spacecraft to the Sun. In contrast to previous work,<sup>13</sup> Eq. (6) is computed given the actual position of the Sun to

account for the inclination of the synodic plane relative to the ecliptic. In practice, one can easily compute the geocentric position of the Sun in the Earth-centered inertial (ECI) coordinate system following the algorithm in Reference 14. A coordinate transformation that includes the rotation matrices  $\mathbf{R}_3(t)$  and  $\mathbf{R}_1(i)$  relate the relative orientation between the ECI and synodic frames\*. Hereunder, a translation by 4,671 km, equivalent to  $l^*\mu$ , shifts the origin of the rotating reference frame to the Earth-Moon barycenter.

$$\begin{bmatrix} x_s \\ y_s \\ z_s \end{bmatrix} = \frac{1}{l^*} \mathbf{R}_3(t) \mathbf{R}_1(i) \begin{bmatrix} X_s \\ Y_s \\ Z_s \end{bmatrix} - \frac{1}{l^*} \begin{bmatrix} 4,671 \text{ km} \\ 0 \\ 0 \end{bmatrix} \quad (7)$$

where  $i$  is the inclination of the orbit of the Moon with respect to the equator corresponding to  $28.59^\circ$ , while  $t$  is the non-dimensional time. The coordinates  $[X_s \ Y_s \ Z_s]^T$  denote the ECI position of the Sun in dimensional units readily available from Reference 14. Therefore, given the synodic position vector of the Sun by Eq. (7), the pseudo-potential function  $\Lambda^*$  that includes the non-dimensional gravitational effect of the Sun is computed.

### Eccentricity Effect of the Moon's Orbit

To account for the true eccentricity of the orbit of the Moon, the difference in the magnitude of the circular and elliptic orbits acting on the spacecraft is modeled through the two-body equations of motion in the ECI coordinate system.<sup>1</sup> Given the initial conditions of the SPO in the synodic frame, one can follow the inverse of the coordinate transformation discussed in the previous section to obtain the required initial position in inertial coordinates. On the other hand, the *rate of change transport theorem* is conveniently used to obtain the initial geocentric velocity.<sup>15</sup> Then, the orbit of the spacecraft around the Earth is simulated with a circular Moon perturbing its orbit to replicate the CR3BP dynamics. However, another Moon with an eccentricity of  $e = 0.0549$ , whose gravitational effect does not perturb the spacecraft trajectory, is added to the simulation. The difference in the magnitudes of the acceleration of the circular and elliptic orbits acting on the spacecraft is computed to model the magnitude of the acceleration perturbing the CR3BP dynamics due to its orbital eccentricity. A conservative approach considering the maximum of this value for one sidereal month is used for simplicity. In this context, the perturbing acceleration, as measured by a synodic observer, due to the eccentricity of the orbit of the Moon becomes the following:

$$\mathbf{a}_{ecc} = -a_{ecc} [\cos(\theta_{ecc}) \quad \sin(\theta_{ecc}) \quad 0]^T \quad (8)$$

where  $a_{ecc}$  denotes the norm of the maximum differential acceleration between the circular and elliptic orbits of the Moon, while  $\theta_{ecc}$  represents the true anomaly of the elliptic orbit of the Moon obtained from Kepler's equation  $M = E - e \sin(E)$ . Here,  $M$  is the mean anomaly while  $E$  denotes the eccentric anomaly. Using Newton's method, one can easily solve for  $E$ :<sup>17</sup>

$$\tan\left(\frac{\theta_{ecc}}{2}\right) = \sqrt{\frac{1+e}{1-e}} \tan\left(\frac{E}{2}\right) \quad (9)$$

---

\*For explicitness,  $\mathbf{R}_1(\cdot)$  and  $\mathbf{R}_3(\cdot)$  denote the Euler rotation matrices about the first and third axes, respectively.<sup>15,16</sup>

Consequently, given the maximum differential acceleration between the circular and elliptic orbits of the Moon, one can easily approximate the perturbation of the eccentricity of the orbit of the Moon within the synodic frame of the CR3BP.

### Solar Radiation Pressure

The cannonball model is employed to describe the Solar radiation pressure (SRP) acceleration of a spherical spacecraft of 1 m in radius and 14 kg of mass:<sup>14</sup>

$$\mathbf{a}_{srp} = -\frac{W A_{s/c} C_R}{cm} \left( \frac{\text{AU}}{r_{s-s/c}} \right)^2 \hat{\mathbf{e}}_{s-s/c} \quad (10)$$

For this, a constant value of the Solar irradiance from the Sun is assumed ( $W = 1367 \text{ W/m}^2$ ).<sup>17</sup> Furthermore, the optical properties of the surface of the spacecraft are assumed to correspond to the intermediate point between a black body and a perfectly reflective surface resulting in a reflection coefficient of  $C_R = 1.5$ . In contrast to other SRP models, the cannonball model conveniently approximates the SRP acceleration of a spacecraft independently of its attitude given the unitary position vector of the Sun relative to the spacecraft  $\hat{\mathbf{e}}_{s-s/c}$ . In this expression,  $c$  denotes the speed of light in the vacuum, AU represents one astronomical unit equivalent to 149,597,870 km,  $A_{s/c}$  is the exposed area of the spacecraft to sunlight, while  $m$  denotes its mass.

### Combined Perturbed System

Ultimately, the equations of motion of the spacecraft include the gravitational pull of the Sun, the SRP acceleration, as well as the effect of the eccentricity of the true orbit of the Moon as follows:

$$\ddot{x} = 2\dot{y} + \frac{\partial \Lambda^*}{\partial x} + a_{srp}^x + a_{ecc}^x \quad \ddot{y} = -2\dot{x} + \frac{\partial \Lambda^*}{\partial y} + a_{srp}^y + a_{ecc}^y \quad \ddot{z} = \frac{\partial \Lambda^*}{\partial z} + a_{srp}^z \quad (11)$$

Such a set of equations are utilized to perturb the SPO of interest and explore the implementation of a variety of control schemes to counteract unmodeled dynamics at the time of computing, i.e., observational time of the Solar corona. Three different control classes are considered to independently address performance in term of robustness, fuel consumption, and complexity: (1) linear state-feedback control, (2) adaptive control, and (3) optimal control.

### LINEAR STATE-FEEDBACK CONTROL LAW

A customary linear state-feedback control policy is initially introduced to track the unperturbed trajectory. Given a nonlinear system within the neighborhood of an equilibrium point, a Taylor series expansion provides a valid linear representation of the dynamics of the system for control implementation.

### Motion Near Equilateral Libration Points

Given a small deviation from the equilibrium point, one can linearize the dynamics of the CR3BP through a Taylor series expansion. In this sense, the equations of motion near equilateral Libration points become the following.<sup>11</sup>

$$\begin{bmatrix} \delta \dot{\mathbf{r}}(t) \\ \delta \ddot{\mathbf{r}}(t) \end{bmatrix} = \begin{bmatrix} 0_{3 \times 3} & I_{3 \times 3} \\ A_{21} & A_{22} \end{bmatrix} \begin{bmatrix} \delta \mathbf{r}(t) \\ \delta \dot{\mathbf{r}}(t) \end{bmatrix} + \begin{bmatrix} 0_{3 \times 3} \\ I_{3 \times 3} \end{bmatrix} \mathbf{u}(t) \quad (12)$$

where  $I_{3 \times 3}$  and  $0_{3 \times 3}$  are the identity and zero matrices, respectively. The term  $\mathbf{u}(t) \in \mathfrak{R}^{3 \times 1}$  corresponds to the control input or propulsive acceleration, while  $\delta \mathbf{r}(t)$  and  $\delta \dot{\mathbf{r}}(t)$  correspond to the relative position and velocity vectors of the spacecraft with respect to the Libration point of interest. It is assumed that the spacecraft has independent control over all axes using conventional ion thrusters.<sup>18</sup> Moreover,  $A_{21}$  and  $A_{22}$  are defined as

$$A_{21} = \begin{bmatrix} 3/4 & -\nu & 0 \\ -\nu & 9/4 & 0 \\ 0 & 0 & -1 \end{bmatrix} \quad A_{22} = \begin{bmatrix} 0 & 2 & 0 \\ -2 & 0 & 0 \\ 0 & 0 & 0 \end{bmatrix} \quad (13)$$

where  $\nu = \pm \frac{3\sqrt{3}}{2}(\mu - 1/2)$  is an auxiliary variable used to facilitate readability. The sign ambiguity in this parameter accounts for the symmetry observed in the CR3BP. A positive value of  $\nu$  denotes linearization around  $L_4$  while a negative value describes the motion about  $L_5$ .<sup>11</sup> Henceforth, SPOs in the vicinity of  $L_4$  are only considered in this study. For simplicity, the linearized system is rewritten in the following compact form.

$$\delta \dot{\mathbf{x}}(t) = A \delta \mathbf{x}(t) + B \mathbf{u}(t) \quad (14)$$

where  $\delta \mathbf{x}(t) \triangleq [\delta \mathbf{r} \quad \delta \dot{\mathbf{r}}]^T$  denotes the relative states of the spacecraft with respect to  $L_4$ . Note that, within the Earth-Moon rotating frame of the CR3BP,  $L_4$  is a stationary point in space; therefore, the relative velocity and acceleration of the spacecraft are equivalent to their absolute values as measured by a synodic observer. Thus, only the relative position of the spacecraft must be carefully computed as follows:

$$\delta \mathbf{r}(t) = \mathbf{r}(t) - \mathbf{r}_{L_4} \quad (15)$$

where  $\mathbf{r}_{L_4}$  denotes the position vector of  $L_4$ .

### Linear Quadratic Tracker

Given the linearized system (Equation (14)), the optimal control policy that minimizes the following performance index function is obtained by solving for the customary Euler-Lagrange equations.<sup>19,20</sup>

$$J = \frac{1}{2} \delta \mathbf{e}^T(T) S(T) \delta \mathbf{e}(T) + \int_0^T \frac{1}{2} \{ \delta \mathbf{e}^T(t) Q \delta \mathbf{e}(t) + \mathbf{u}^T(t) R \mathbf{u}(t) \} dt \quad (16)$$

Here,  $Q \in \mathfrak{R}^{6 \times 6}$  and  $R \in \mathfrak{R}^{3 \times 3}$  are positive definite weight matrices used to penalize tracking against propulsive acceleration, respectively. Henceforth,  $\delta \mathbf{x}_r(t)$  denotes the reference unperturbed trajectory relative to  $L_4$ , while  $\delta \mathbf{e}(t) \triangleq \delta \mathbf{x}(t) - \delta \mathbf{x}_r(t)$  is the relative tracking error.

As it is commonly known from the literature, the solution to this optimal control problem, referred to as the LQ tracker, results in a linear time-varying (finite-horizon) state-feedback control policy

giving the solution to the Matrix Riccati Equation  $S(t)$ .<sup>19,20</sup> However, assuming the final non-dimensional time  $T$  is sufficiently large to allow for convergence to the reference trajectory, a constant gain (infinite horizon) state-feedback control policy ensures an approximate solution to the optimal control problem as long as the pair  $(A, B)$  is stabilizable and  $(A, \sqrt{Q})$  is observable.<sup>19,20</sup> In this sense, the optimal control policy becomes the following.

$$\mathbf{u}(t) = -R^{-1}B^T S_\infty \delta \mathbf{x}(t) + R^{-1}B^T \mathbf{v}(t) \quad (17)$$

where  $S_\infty$  is the solution to the Algebraic Riccati Equation given the state and input matrices  $A$  and  $B$ , respectively. The second term in Equation (17) represents the feed-forward signal required to track the reference trajectory. Here,  $\mathbf{v}(t)$  is commonly integrated offline backwards in time given its respective dynamics and terminal condition as follows:

$$\dot{\mathbf{v}}(t) = -(A - BK_\infty)^T \mathbf{v}(t) - Q\delta \mathbf{x}_r(t) \quad s.t. \quad \mathbf{v}(T) = S(T)\delta \mathbf{x}_r(T) \quad (18)$$

where  $K_\infty = R^{-1}B^T S_\infty$  is the LQR control gain matrix. However, as  $A - BK_\infty$  is by design Hurwitz,  $\dot{\mathbf{v}}(t) \rightarrow 0$  as  $t \rightarrow \infty$ . In this sense, a convenient expression for online implementation of  $\mathbf{v}(t)$  is obtained as follows:<sup>19,20</sup>

$$\mathbf{v}(t) = -(A - BK_\infty)^{-T} Q\delta \mathbf{x}_r(t) \quad (19)$$

Even though the LQ tracker does not account for unknown perturbations as well as the nonlinearities of the actual dynamics, it guarantees a locally stable closed-loop system. In the following section, an MRAC with disturbance rejection is derived to estimate unknown disturbances for a more robust control technique while proving global asymptotic tracking.

## ADAPTIVE CONTROL

As a means to increase robustness and prove global asymptotic stability of the closed-loop nonlinear dynamics, an MRAC with disturbance rejection is derived in this section. Furthermore, such formulation is modified with an  $\mathcal{L}_1$ -type adaptive control architecture to guarantee fast convergence of the estimated perturbations.

### Model Reference Adaptive Control with Disturbance Rejection

Following Reference 10, the perturbed dynamics are rewritten in the following form to independently manipulate the linearities, nonlinearities, and perturbations of the system:

$$\dot{\mathbf{x}}(t) = L\mathbf{x}(t) + B(\mathbf{f}(t) + \mathbf{p}(t) + \mathbf{u}(t)) \quad (20)$$

where  $\mathbf{x}(t) \triangleq [\mathbf{r}(t) \quad \dot{\mathbf{r}}(t)]^T$  denotes the state of the spacecraft,  $\mathbf{p}(t) \in \mathbb{R}^{3 \times 1}$  represents the unmodeled and unknown orbital perturbations, and  $L \in \mathbb{R}^{6 \times 6}$  and  $\mathbf{f}(t) \in \mathbb{R}^{3 \times 1}$  denote the linear and nonlinear domains of the CR3BP explicitly defined in the Appendix. Similarly, the reference unperturbed system is written as follows:

$$\dot{\mathbf{x}}_r(t) = L\mathbf{x}_r(t) + B\mathbf{f}_r(t) \quad (21)$$

Henceforth, all variables denoted by the subscript  $r$  correspond to the reference unperturbed model. Furthermore, as the trajectory of the spacecraft along its SPO is periodic, gravitational perturbations are modeled as a linear combination of sinusoidal basis functions at a certain frequency. In this sense,  $\mathbf{p}(t)$  becomes:

$$\mathbf{p}(t) = \Theta\phi(t) \quad (22)$$

where  $\Theta \in \mathbb{R}^{3 \times n}$  is a matrix of unknown constant coefficients and  $\phi(t) \in \mathbb{R}^{n \times 1}$  is a vector of orthogonal user-defined basis functions. Here,  $n$  denotes the number of basis functions. The control objective is to design an adaptive control policy that estimates the matrix of unknown coefficients  $\Theta$  required to cancel out the effect that perturbations have on the system. Also,  $\mathbf{x}(t) \rightarrow \mathbf{x}_r(t)$  as  $t \rightarrow \infty$ . As common practice, a positive definite radially unbounded scalar value Lyapunov candidate function is defined as follows:

$$V(t) = \frac{1}{2}\mathbf{e}(t)^T\Omega\mathbf{e}(t) + \frac{1}{2}\text{tr}(\Delta\Theta^T(t)\Pi^{-1}\Delta\Theta(t)) > 0 \quad \forall \quad \mathbf{e}(t), \Delta\Theta(t) \neq 0 \quad (23)$$

where  $\mathbf{e}(t) \triangleq \mathbf{x}(t) - \mathbf{x}_r(t)$  and  $\Delta\Theta(t) \triangleq \hat{\Theta}(t) - \Theta$  are the tracking and estimation error, respectively.  $\Pi \in \mathbb{R}^{n \times n}$  is positive definite matrix used to adjust the adaptation rate of the estimated parameters. On the other hand,  $\Omega \in \mathbb{R}^{6 \times 6}$  is a positive definite matrix used prove global asymptotic stability. Here,  $\hat{\Theta}(t)$  is the matrix of estimated coefficients. Since the estimation error is a matrix, the *trace* operator  $\text{tr}(\cdot)$  is used to guarantee a positive scalar term in the Lyapunov candidate function. From here, assuming the uncertain parameters in  $\Theta$  are constant, the tracking and estimation errors are differentiated:

$$\dot{\mathbf{e}}(t) = \dot{\mathbf{x}}(t) - \dot{\mathbf{x}}_r(t) \quad (24)$$

$$\Delta\dot{\Theta}(t) = \dot{\hat{\Theta}}(t) \quad (25)$$

Consequently, by taking the Lyapunov function first-order time derivative and rearranging after substituting for the tracking and estimation error dynamics, the following is obtained after some algebraic manipulation\*:

$$\dot{V}(t) = \mathbf{e}^T\Omega L\mathbf{e} + \mathbf{e}^T\Omega B(\mathbf{f} - \mathbf{f}_r + \hat{\Theta}\phi + \mathbf{u}) + \text{tr}(\Delta\Theta(\Pi^{-1}\Delta\dot{\Theta}^T - \phi\mathbf{e}^T\Omega B)) \quad (26)$$

The update law is designed by forcing the third term in Equation (26) to be equal to zero in order to remove the estimation error dependency in this expression.

$$\dot{\hat{\Theta}}(t) = B^T\Omega\mathbf{e}(t)\phi(t)\Pi \quad (27)$$

Furthermore, the control policy is designed as follows:

$$\mathbf{u}(t) = -K\mathbf{e}(t) - \hat{\Theta}(t)\phi(t) - (\mathbf{f}(t) - \mathbf{f}_r(t)) \quad (28)$$

---

\*Time arguments for time-varying variables in Equation (26) are ignored for clarity.

where  $K$  is a control gain matrix designed such that  $L - BK$  is Hurwitz. Therefore,  $\dot{V}$  becomes the following:

$$\dot{V}(t) = e^T(t)\Omega(L - BK)e(t) \quad (29)$$

From here,  $\Omega > 0$  is designed under the condition that  $\Omega(L - BK) = -\Upsilon$  where  $\Upsilon$  is a positive definite matrix. This ensures a Lyapunov semi-definite time derivative, which initially proves boundedness of the augmented states using Lyapunov's direct method.<sup>21</sup>

$$\dot{V}(t) = -e^T(t)\Upsilon e(t) \leq 0 \quad (30)$$

The stability conclusions are further extended by invoking Barbalat's Lemma.<sup>21</sup> Barbalat's Lemma states that if the Lyapunov candidate function is bounded and its first-order time derivative is uniformly continuous (e.i.,  $\ddot{V}$  is bounded), then  $\dot{V} \rightarrow 0$  as  $t \rightarrow \infty$ . In this case, this implies that  $e(t) \rightarrow 0$  as  $t \rightarrow \infty$ . Thus, global asymptotic tracking of the states of the spacecraft to its reference SPO is proven. Conversely, given a sufficiently diverse set of basis functions, it is guaranteed convergence of the estimated parameters to any linear combination of the basis functions required to counteract the effect of orbital perturbations.

### $\mathcal{L}_1$ -Type Adaptive Control

The preceding adaptive control formulation is modified with an  $\mathcal{L}_1$ -type adaptive control architecture to guarantee fast convergence of the estimated perturbations for instances in which the initial tracking error is significantly large. Furthermore, the following refinement technique enables the likelihood to transition between a family of SPOs to maximize eclipse time while still estimating orbital perturbations without any retuning. This is achieved as a consequence of the following state predictor and control law:<sup>22</sup>

$$\hat{\mathbf{x}}(t) = L\mathbf{x}(t) + B(\mathbf{f}(t) + \mathbf{u}_2(t) + \hat{\mathbf{p}}(t)) + A_m\mathbf{e}(t) \quad (31)$$

$$\mathbf{u}(t) = -K\mathbf{e}(t) + \mathbf{u}_2(t) \quad (32)$$

where  $\hat{\mathbf{p}}(t)$  denotes the estimated perturbations and  $A_m \in \mathfrak{R}^{6 \times 6}$  an arbitrary Hurwitz matrix. Here, the second term in Equation (32) represents the adaptive control signal described as follows in the Laplace domain.

$$\mathbf{u}_2(s) = -C(s)\hat{\mathbf{p}}(s) \quad (33)$$

Within this expression,  $C(s) \triangleq \omega/(s + \omega)$  is specified as a low-pass first-order filter of bandwidth  $\omega$ , while  $\hat{\mathbf{p}}(t)$  obeys to the following update law:

$$\dot{\hat{\mathbf{p}}}(t) = B^T\Omega_1\mathbf{e}(t)\Pi_1 \quad (34)$$

where  $\Omega_1$  and  $\Pi_1$  are tuning matrices explicitly defined for the  $\mathcal{L}_1$ -type control formulation. Note that the update law in Equation (34) follows the same structure as in Equation (27); nevertheless, basis functions are not considered as fast adaptation is guaranteed.<sup>22</sup>

## NONLINEAR DYNAMIC PROGRAMMING CONTROL PROBLEM

To further assess the aforementioned feedback control techniques in terms of tracking and fuel consumption, the following nonlinear dynamic programming control problem is solved using the optimal control software *GPOPS-II* along with the interior-point optimizer *IPOPT*.<sup>8</sup> More in detail, *GPOPS-II* transcribes the continuous-time optimal control problem using variable-order Gaussian quadrature methods to a sparse nonlinear programming problem (NLP). In this context, *IPOPT* is used as a NLP solver to determine the optimal control sequence that satisfies user-entered settings. In this study, the optimal control problem is formulated as follows. Minimize the performance index function

$$J = \frac{1}{2} \int_0^T \mathbf{u}^T(t) \mathbf{u}(t) dt \quad (35)$$

subject to the dynamic constraints of algebraic differential equations found in Equation (11) and the following initial conditions:

$$\begin{aligned} x(0) &= x_0 & y(0) &= y_0 & z(0) &= z_0 \\ \dot{x}(0) &= \dot{x}_0 & \dot{y}(0) &= \dot{y}_0 & \dot{z}(0) &= \dot{z}_0 \end{aligned} \quad (36)$$

Terminal conditions are free while the following inequality constraints must hold at all times\*:

$$0 \leq \| \mathbf{u}(t) \| \leq u_{max} \quad (37)$$

$$0 \leq x - x_r \leq \Delta_{max} \quad 0 \leq y - y_r \leq \Delta_{max} \quad 0 \leq z - z_r \leq \Delta_{max} \quad (38)$$

This ensures the control sequence does not exceed the physical limits of the propulsion system, while constraining the allowable position error ( $\Delta_{max}$ ) to a user-defined maximum value from its reference SPO. For explicitness,  $\| \mathbf{u}(t) \|$  denotes the euclidean norm of the propulsive acceleration, while  $u_{max}$  represents its maximum value. Note that the inequality constraints in Equation (38) independently describe the allowable position tracking error along each axis. This ensures the convergence of the algorithm to a solution while avoiding numerical limitations. Indeed, each constraint in Equation (38) is intentionally lower bounded by zero to only allow positive values of the position tracking error.

In this formulation, the mass of the spacecraft is assumed to remain constant. In practice,  $\Delta_{max}$  denotes the tolerance of the eclipse zone to perform LO. The performance index function in Equation (35) corresponds to an integral cost that minimizes the propulsive acceleration throughout the entire length of the mission; it describes the mathematical relationship required to minimize fuel consumption. Even though this approach does not feature state-feedback, it offers an approximate solution to the global optimal control problem. A discussion on the initial guess and mesh settings as well as the numerical methods used to converge to a solution are described in the following section.

---

\*The initial time and final time are fixed as this does not correspond to a minimum-time optimal control problem.

## NUMERICAL RESULTS AND DISCUSSION

In this study, three nominal SPOs, adopted from Reference 1, are used to assess the three control classes in terms of fuel consumption and position tracking error (see Figure 2). According to Reference 1, up to 0.8 hours of eclipse time is anticipated per orbital period on average. A mission of 38 sidereal months of duration is proposed by the authors to address any scientific objectives of interest. The results of this paper are numerically obtained using *Matlab*. Design parameters for all control schemes are presented in the Appendix. In this sense, the mean position tracking error is computed and presented in Table 1. Furthermore, assuming the mass of the spacecraft remains constant throughout the entire duration of the mission, the fuel consumption in terms of  $\Delta V$  is reported in Table 2. The set of basis functions, required by the adaptive control formulation, are numerically obtained offline by a nonlinear least-square fit of the time-history of the orbital perturbations acting on the spacecraft. A regression model of sinusoids at different unknown frequencies is used for simplicity for an arbitrary SPO. The same set of sinusoidal basis functions are employed for all three SPOs analyzed in this study. Therefore, sine and cosine functions at the following frequencies are used as basis functions:  $\{0.9988 \text{ rad}, 1.8400 \text{ rad}, 0.0131 \text{ rad}, 0.8411 \text{ rad}\}$ .\*

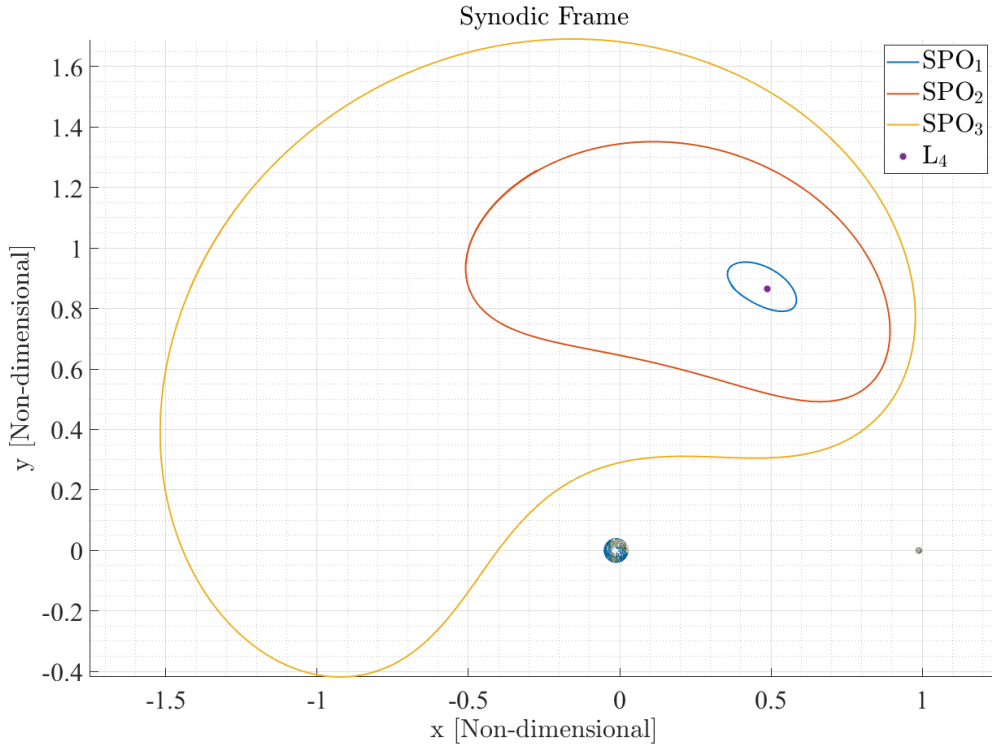


**Figure 2. Short-Period Orbits of Interest Adopted from Reference 1.**

---

\*Note that these values are in radians and not in radians per second as the non-dimensional time is used as the independent variable.

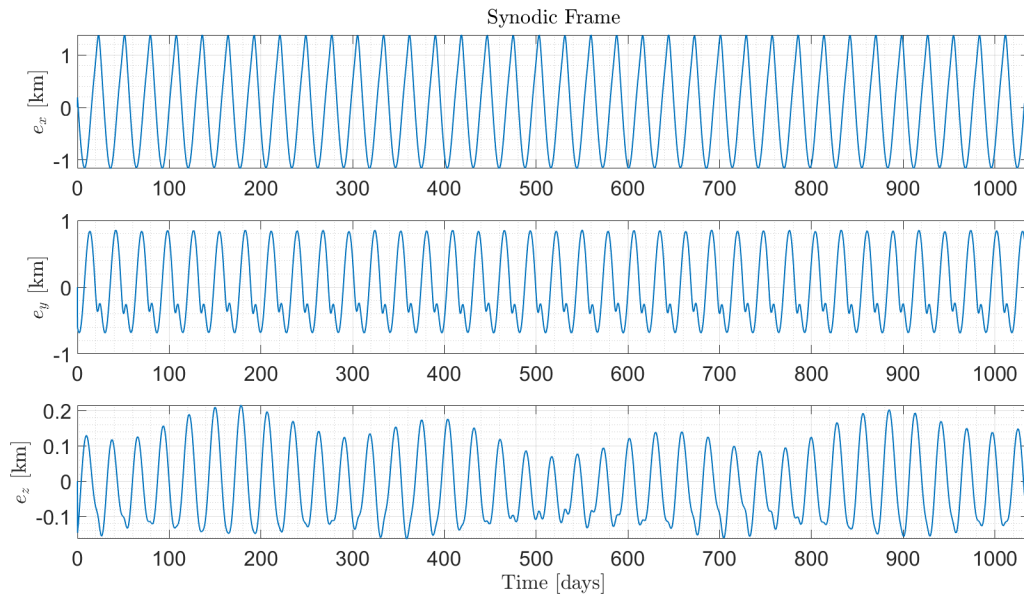
**Table 1. Mean Position Tracking Error [km]**

Orbit	LQT	MRAC	$\mathcal{L}_1$ -Type	NLP
SPO <sub>1</sub>	0.17	$2.89 \times 10^{-4}$	0.14	0.09
SPO <sub>2</sub>	0.96	$3.87 \times 10^{-4}$	0.25	0.09
SPO <sub>3</sub>	1.97	$4.30 \times 10^{-4}$	0.29	0.09

**Table 2. Fuel Consumption Requirements ( $\Delta V$ ) [km/s]**

Orbit	LQT	MRAC	$\mathcal{L}_1$ -Type	NLP
SPO <sub>1</sub>	2.21	2.21	2.21	2.30
SPO <sub>2</sub>	3.39	3.39	3.39	3.42
SPO <sub>3</sub>	3.89	3.89	3.89	3.82

For demonstration purposes, the time evolution of the position tracking error and the required propulsive acceleration are presented for each control strategy for SPO<sub>2</sub> (see Figure 4 - Figure 11). While all three control formulations offer applicable results to perform LO, it is found that all state-feedback control policies virtually feature equivalent fuel consumption requirements to stay in orbit. Indeed, as shown in Figure 4, Figure 6, and Figure 9, the time history of the propulsive acceleration exhibits a similar profile. Nevertheless, as shown in Figure 5, the MRAC formulation offers better tracking as perturbations are continuously being estimated to stay in orbit.

**Figure 3. Time Evolution of the Position Tracking Error of SPO<sub>2</sub> under LQT Control Law.**

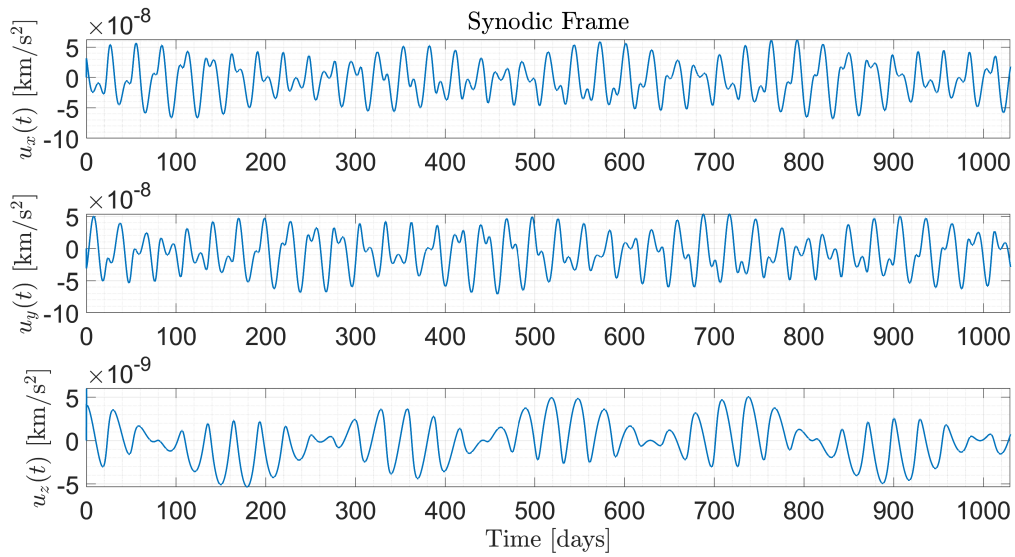


**Figure 4. Time Evolution of the Propulsive Acceleration of SPO<sub>2</sub> under LQT Control Law.**

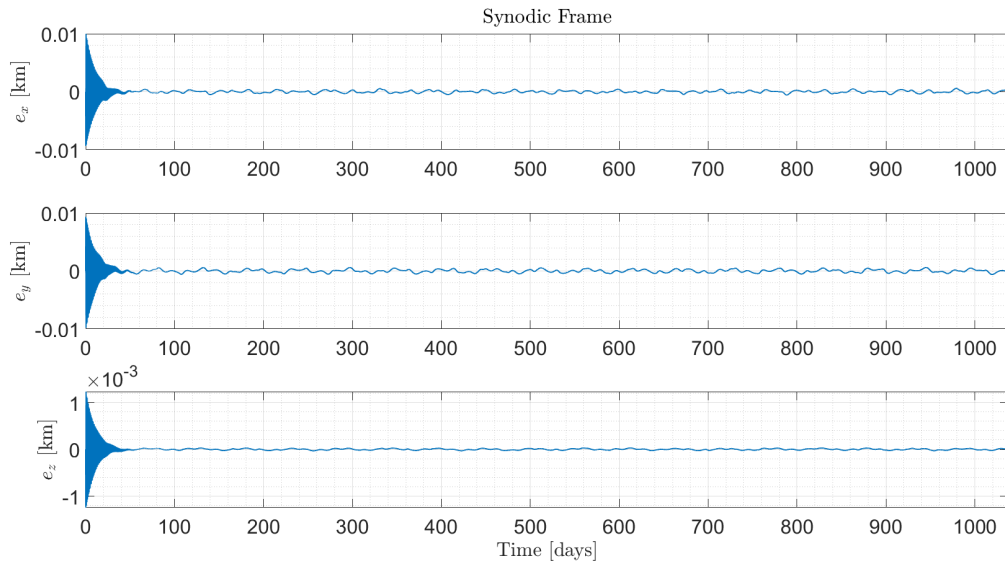


**Figure 5. Time Evolution of the Position Tracking Error of SPO<sub>2</sub> under MRAC Control Policy.**

Figure 7 presents the time evolution of the estimated perturbations along with their actual values. For simplicity, all estimated parameters are initialized to zero. A closeup view by Figure 8 reveals the transient response of the estimates. As guaranteed by the stability proof, the update law given by Equation 27 finds any linear combination of the basis functions to accurately estimate the perturbations within one orbital period. Nevertheless, the  $\mathcal{L}_1$ -type adaptive control formulation results in a more robust approach due to its architecture. As shown in Figure 9 and Figure 10, this method exhibits comparable performance relative to the aforementioned control schemes. In addition, Figure 11 demonstrates fast convergence relative to a traditional MRAC.

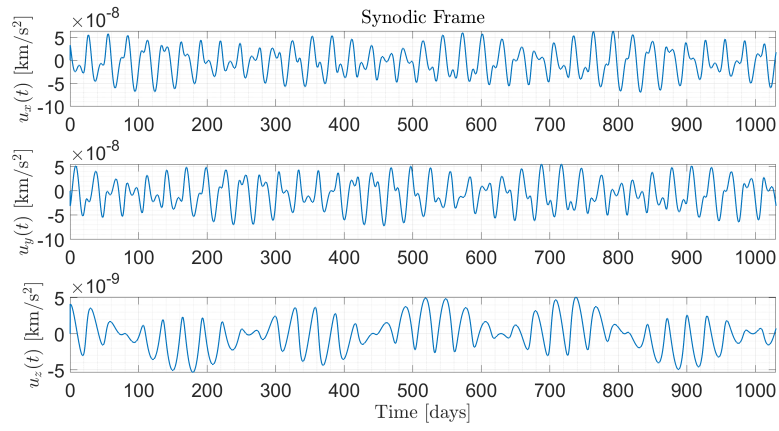


**Figure 6. Time Evolution of the Propulsive Acceleration of SPO<sub>2</sub> under MRAC Control Policy.**

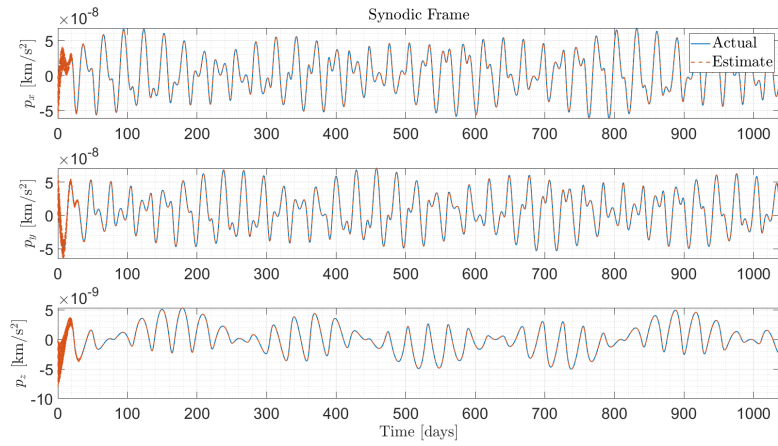


**Figure 7. Time Evolution of the Estimated Perturbations of SPO<sub>2</sub> under MRAC Update Law.**

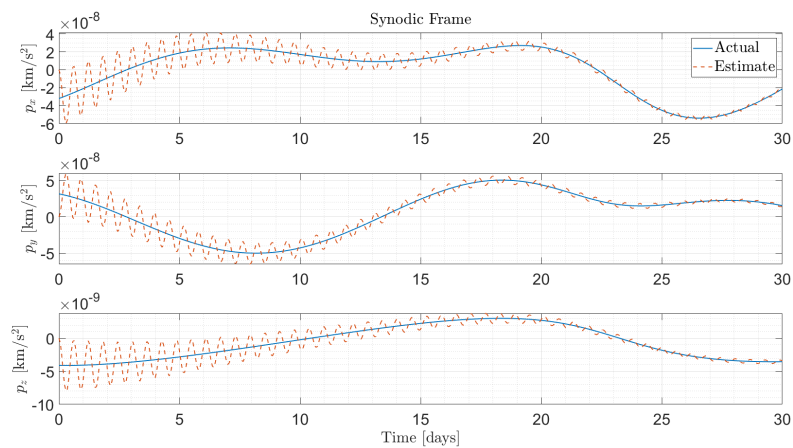


**Figure 8. Close-Up View of the Estimated Perturbations of SPO<sub>2</sub> under MRAC Update Law.**

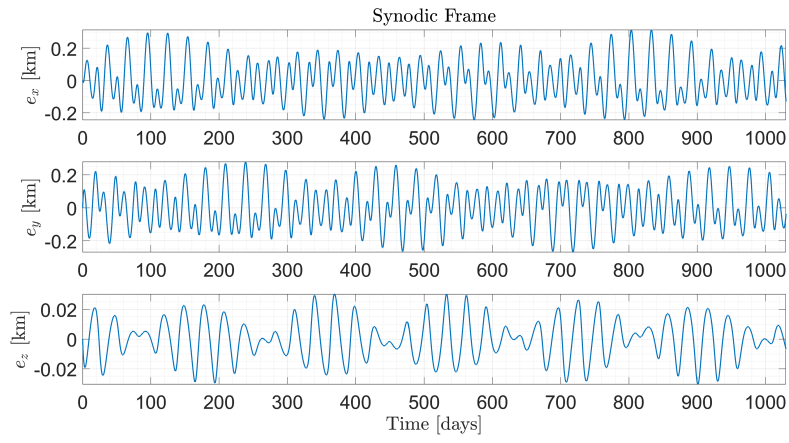


**Figure 9. Time Evolution of the Position Tracking Error of SPO<sub>2</sub> under  $\mathcal{L}_1$  Control Policy.**

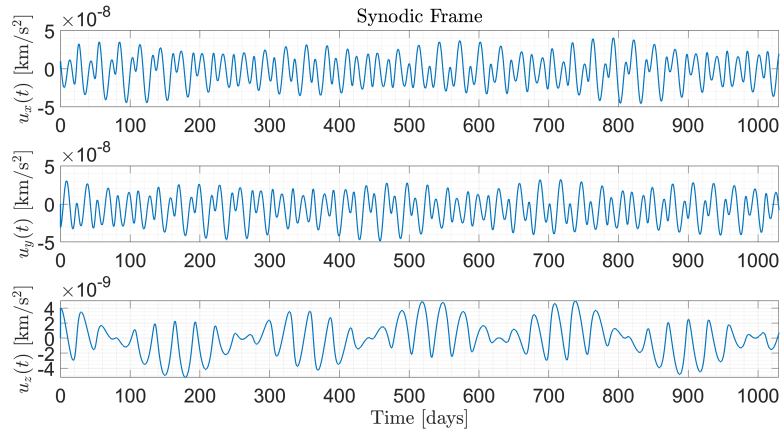


**Figure 10. Time Evolution of the Propulsive Acceleration of SPO<sub>2</sub> under  $\mathcal{L}_1$  Control Policy.**

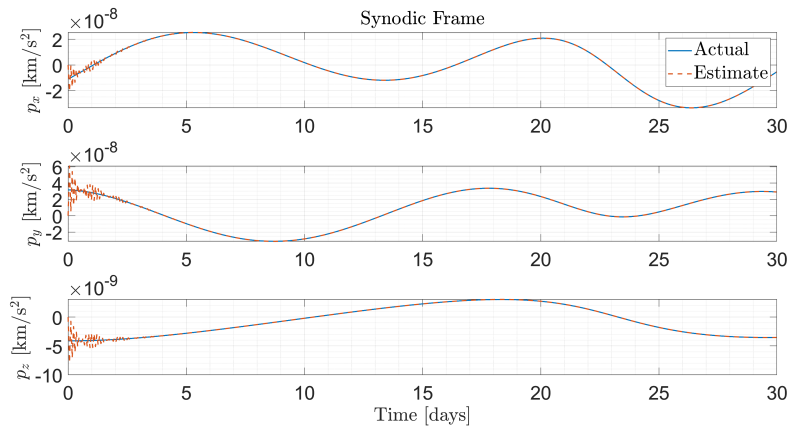


**Figure 11. Close-Up View of the Estimated Perturbations of SPO<sub>2</sub> under  $\mathcal{L}_1$  Control formulation.**

As the preceding control methods feature the same performance, the result are validated by comparing to an approximation of the global fuel-optimal solution using the *GPOPS-II* along with the *IPOPT* solver. For this, a multiple-stage approach allows for convergence by discretizing the time domain into number of orbits. For  $SPO_1$  and  $SPO_2$ , optimal solutions are found every two orbits. Conversely, for  $SPO_3$ , the optimal control software converges to a solution after each orbit. For this, the unperturbed systems is used as the initial guess while a second-order sparse central difference method is set as the derivative supplier. The mesh tolerance is adjusted to  $10^{-8}$  for  $SPO_1$  and  $SPO_2$  while this value is set to  $10^{-4}$  for  $SPO_3$  due to numerical limitations. Results presented in Table 1 and Table 2 indicate that the state-feedback control methods are comparable with the fuel-optimal solution in terms of  $\Delta V$  and position tracking error. This concludes that an approximation of the fuel-optimal control problem is achievable with any of the state-feedback control strategies discussed in this paper. For a visual representation of the optimal control solution, Figure 12 shows the time evolution of the position tracking error given the control sequence in Figure 13.

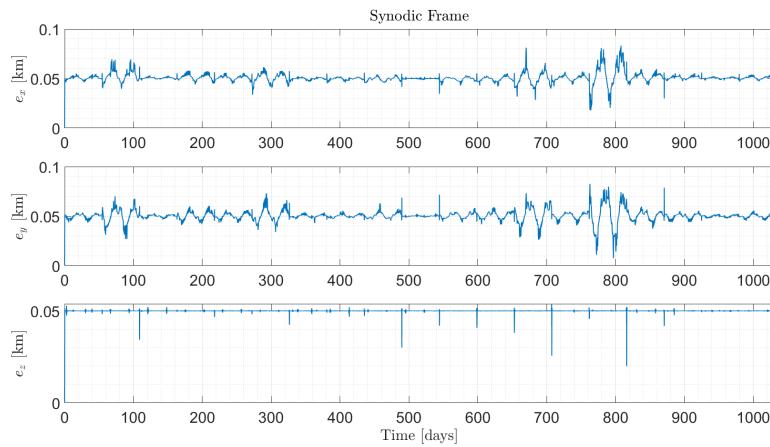


**Figure 12. Time Evolution of the Fuel-Optimal Position Tracking Error.**

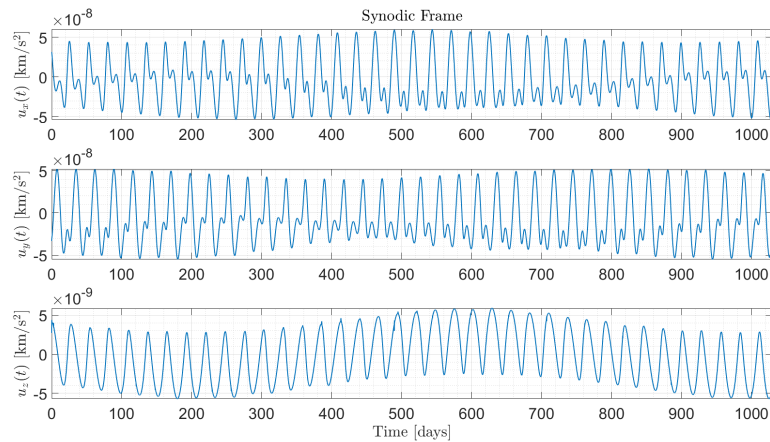


**Figure 13. Time Evolution of the Fuel-Optimal Control Sequence.**

Overall, the results of this paper meet with the tracking requirements of each SPO to perform LO. Moreover, all control policies do not exceed the physical limits of modern ion propulsion system in terms of maximum acceleration.<sup>18</sup> Similarly, fuel-consumption requirements are kept within the limits of recent missions in the Cislunar region. For instance, ion propulsion systems for 6U CubeSats, recently onboarded the SLS, provide a total  $\Delta V$  of up to 2.9 km/s.<sup>18</sup> Moreover, high-performance CubeSat propulsion systems are capable of up to 5.8 km/s of  $\Delta V$  based on payload.<sup>23</sup>

## CONCLUSIONS

The results of this paper highlight the need to account for orbital perturbations by comparing three different control classes in terms of tracking, fuel consumption, and complexity: (1) linear-state feedback, (2) adaptive control, and (3) optimal control. While all control laws demonstrate feasible tracking with reasonable fuel consumption for a family of SPOs, the  $\mathcal{L}_1$ -type adaptive control architecture suggests a more robust control technique with fast adaptation to the unknown disturbance when compared to the aforementioned control methods. Moreover, the solution to the fuel-optimal nonlinear dynamic programming problem indicates that for any of the state-feedback control strategies discussed in this paper the fuel-optimal control sequence is achievable. Recall that the proposed mission aims to perform LO as an observational technique to study various scientific objectives. The present study proves that perturbations can be effectively mitigated to achieve the science goals.

## ACKNOWLEDGMENTS

The authors acknowledge the help and support from the Space Trajectories and Applications Research (STAR) and Advanced Autonomous Multiple Spacecraft (ADAMUS) research groups at Embry-Riddle Aeronautical University, Daytona Beach. In particular, the authors acknowledge the support from Emanuela Gaglio and Dr. Jhonathan Murcia Piñeros for their judgement and experience in nonlinear dynamic programming. Drs. Fors and Gómez acknowledge the support by the Spanish Ministerio de Ciencia e Innovación (MICINN) under grant PID2021-125627OB-C31 and through the “Center of Excellence María de Maeztu 2020-2023” award to the ICCUB (CEX2019-000918-M). Dr. Fors also acknowledges the support by the Spanish Ministerio de Ciencia e Innovación (MICINN) under grant PID2019-105510GB-C31.

## APPENDIX: MODIFIED REPRESENTATION OF THE PERTURBED CR3BP

The equations of motion of a spacecraft under the perturbed CR3BP may be rewritten in the following manner after analytically computing the gradient of the pseudo-potential function in Equation (2).

$$\ddot{x} = 2\dot{y} + x - \frac{(1-\mu)(x+\mu)}{r_{e-s/c}^3} - \frac{\mu(x-1-\mu)}{r_{m-s/c}^3} + p_x(t) \quad (39a)$$

$$\ddot{y} = -2\dot{x} + y - \frac{(1-\mu)y}{r_{e-s/c}^3} - \frac{\mu y}{r_{m-s/c}^3} + p_y(t) \quad (39b)$$

$$\ddot{z} = -\frac{\mu z}{r_{m-s/c}^3} + p_z(t) \quad (39c)$$

where  $\mathbf{p}(t) = [p_x(t) \ p_y(t) \ p_z(t)]^T$  denotes the orbital perturbations along the coordinates of the Earth-Moon rotating frame. In this sense, the linear terms are collected in the following form while any remaining nonlinearities are denoted by  $\mathbf{f}(t) = [f_x(t) \ f_y(t) \ f_z(t)]^T$ .

$$\dot{\mathbf{x}}(t) = L\mathbf{x}(t) + B(\mathbf{f}(t) + \mathbf{p}(t)) \quad (40)$$

where  $L$  is defined as follows:

$$L = \begin{bmatrix} 0_{3 \times 3} & I_{3 \times 3} \\ L_{21} & L_{22} \end{bmatrix} \quad (41)$$

Furthermore, the partitioned matrices  $L_{21}$  and  $L_{22}$  are given by

$$L_{21} = \begin{bmatrix} 1 & 0 & 0 \\ 0 & 1 & 0 \\ 0 & 0 & 0 \end{bmatrix} \quad L_{22} = \begin{bmatrix} 0 & 2 & 0 \\ -2 & 0 & 0 \\ 0 & 0 & 0 \end{bmatrix} \quad (42)$$

while the nonlinear terms are the following:

$$f_x = -\frac{(1-\mu)(x+\mu)}{r_{e-s/c}^3} - \frac{\mu(x-1-\mu)}{r_{m-s/c}^3} \quad (43a)$$

$$f_y = -\frac{(1-\mu)y}{r_{e-s/c}^3} - \frac{\mu y}{r_{m-s/c}^3} \quad (43b)$$

$$f_z = -\frac{\mu z}{r_{m-s/c}^3} \quad (43c)$$

## APPENDIX: DESIGN CONTROL PARAMETERS

All necessary design control parameters are reported in Table 3. For clarity,  $diag[\cdot]$  denotes a diagonal matrix whose elements are given by its argument.

**Table 3. Design Control Parameters**

Symbol	Value
$A_m$	$-10I_{6 \times 6}$
$R$	$I_{3 \times 3}$
$Q$	$[1 \times 10^{22}diag[1, 1, 1 \times 10^{-14}]; 1 \times 10^3 I_{3 \times 3}]$
$\Pi$	$1 \times 10^5 I_{8 \times 8}$
$\Pi_1$	$1 \times 10^8$
$\Upsilon$	$I_{6 \times 6}$
$\omega$	1

\*Recall  $\mathbf{x}(t)$  denotes the states of the spacecraft.

## REFERENCES

- [1] K. Patel, L. E. Mendoza Zambrano, D. Canales, R. Bevilacqua, S. Eikenberry, O. Fors, J. M. Gómez, and A. Richichi, “Controlled Short-Period Orbits Around Earth-Moon Equilateral Libration Points for Lunar Occultations,” *Acta Astronautica*, Vol. 211, October 2023, pp. 781–794, <https://doi.org/10.1016/j.actaastro.2023.07.015>.
- [2] S. Doroba, R. Kale, D. Canales, H. Cho, S. Eikenberry, O. Fors, J. M. Gomez, and A. Richichi, “Leveraging the Moon and Stable Libration Point Orbits Around L4/L5 to Observe the Solar Corona,” *33<sup>rd</sup> AAS/AIAA Spaceflight Mechanics Meeting*, Austin, Texas, January 2023. Paper AAS-23-326.
- [3] A. Richichi, “Lunar Occultations: From Past to Future Achievements,” *Symposium-International Astronomical Union*, Vol. 158, 1994, pp. 71–81, <https://doi.org/10.1017/S0074180900107338>.
- [4] V. Szebehely, *Theory of Orbits: The Restricted Problem of Three Bodies*, Vol. 13. 111 5<sup>th</sup> Avenue, New York, NY: Academic Press, 1967, <https://doi.org/10.1016/B978-0-12-395732-0.X5001-6>.
- [5] C. Gao, J. J. Masdemont, G. Gómez, J. Chen, and J. Yuan, “High Order Dynamical Systems Approaches for Low-Thrust Station-Keeping of Libration Point Orbits,” *Acta Astronautica*, Vol. 190, January 2022, pp. 349–364, <https://doi.org/10.1016/j.actaastro.2021.10.015>.
- [6] T. Pavlak and K. Howell, “Strategy for Optimal, Long-Term Stationkeeping of Libration Point Orbits in the Earth-Moon System,” *AIAA/AAS Astrodynamics Specialist Conference*, 2012. Paper AAS11-516.
- [7] Y. Jin and B. Xu, “A Modified Targeting Strategy for Station-Keeping of Libration Point Orbits in the Real Earth-Moon System,” *International Journal of Aerospace Engineering*, Vol. 2019, 2019, <https://doi.org/10.1155/2019/3257514>.
- [8] M. A. Patterson and A. V. Rao, “GPOPS-II: A MATLAB Software for Solving Multiple-Phase Optimal Control Problems Using Hp-Adaptive Gaussian Quadrature Collocation Methods and Sparse Nonlinear Programming,” *ACM Trans. Math. Softw.*, Vol. 41, October 2014, <http://dx.doi.org/10.1145/2558904>.
- [9] N. Hovakimyan and C. Cao,  *$\mathcal{L}_1$  Adaptive Control Theory: Guaranteed Robustness with Fast Adaptation*. Advances in Design and Control, United Kingdom: Cambridge University Press, 2010, <https://doi.org/10.1137/1.9780898719376>.
- [10] N. T. Nguyen, *Model-Reference Adaptive Control*. Gewerbstrasse 11, 6330 Cham, Switzerland: Springer, 2018, [https://doi.org/10.1007/978-3-319-56393-0\\_5](https://doi.org/10.1007/978-3-319-56393-0_5).
- [11] W. Ulrich, *Astronautics: The Physics of Space Flight*. Gewerbstrasse 11, 6330 Cham, Switzerland: Spinger, 3<sup>rd</sup> ed., 2018, <https://doi.org/10.1007/978-3-319-74373-8>.
- [12] P. Wang, X.-J. Jiang, X.-Y. Hou, L.-H. Zhang, L.-X. Jiang, J.-Q. Wang, H. Zhi, Z.-L. Jiao, T. Li, M.-H. Liu, *et al.*, “Ground- and Space-Based Observation of Kordylewski Clouds,” *Space: Science & Technology*, 2021, <https://doi.org/10.34133/2021/6597921>.
- [13] K. K. Boudad, *Trajectory Design Between Cislunar Space and Sun-Earth Libration Points in a Four-Body Model*. PhD thesis, Purdue University, 2022, <https://doi.org/10.25394/PGS.19669632.v1>.
- [14] H. Curtis, *Orbital Mechanics for Engineering Students*. Butterworth-Heinemann, 3<sup>rd</sup> ed., 2014, <https://doi.org/10.1016/C2011-0-69685-1>.
- [15] A. Rao, *Dynamics of Particles and Rigid Bodies: A Systematic Approach*. New York: Cambridge University Press, 2005, <https://doi.org/10.1017/CBO9780511805455>.
- [16] D. C. Garcia, *Transfer Design Methodology Between Neighborhoods of Planetary Moons in the Circular Restricted Three-Body Problem*. PhD thesis, Purdue University, 2021.
- [17] D. A. Vallado, *Fundamentals of Astrodynamics and Applications*. 4940 West 147<sup>th</sup> Street, Hawthorne, CA: Microcosm Press and Springer, 4<sup>th</sup> ed., 2013.
- [18] M. Tsay, J. Model, C. Barcroft, J. Frongillo, J. Zwahlen, and C. Feng, “Integrated Testing of Iodine Bit-3 RF Ion Propulsion System for 6u Cubesat Applications,” *35<sup>th</sup> International Electric Propulsion Conference, Atlanta, USA*, October 2017. Paper IEPC-2017-264.
- [19] F. L. Lewis, D. Vrabie, and V. L. Syrmos, *Optimal control*. 111 River St, Hoboken, NJ: John Wiley & Sons, 3<sup>rd</sup> ed., 2012, <https://doi.org/10.1002/9781118122631>.
- [20] D. E. Kirk, *Optimal Control Theory: An Introduction*. Mineola, NY: Courier Corporation, 2004 - 1970.
- [21] H. Khalil, *Nonlinear Systems*. Upper Saddle River, NJ: Prentice Hall, 3<sup>rd</sup> ed., 2001.
- [22] X. Wang and N. Hovakimyan, “L1 Adaptive Controller for Nonlinear Time-Varying Reference Systems,” *Systems & Control Letters*, Vol. 61, No. 4, 2012, pp. 455–463, <https://doi.org/10.1016/j.sysconle.2012.01.010>.
- [23] S. Samples and R. Wirz, “Parametric Analysis of High-Delta-V Cubesat Missions with a Miniature Ion Thruster,” *Journal of Spacecraft and Rockets*, Vol. 58, May–June 2021, pp. 754–763, <https://doi.org/10.2514/1.A34827>.